Turkish Journal of Chemistry

http://journals.tubitak.gov.tr/chem/

Research Article

Turk J Chem
(2017) 41: 272 – 281

doi:10.3906/kim-1605-50

Activity of γ-Al_2O_3-based Mn, Cu, and Co oxide nanocatalysts for selective catalytic reduction of nitric oxide with ammonia

Parvaneh NAKHOSTIN PANAHI[1,*], **Gérard DELAHAY**[2], **Seyed Mahdi MOUSAVI**[3]
[1]Department of Chemistry, Faculty of Science, University of Zanjan, Zanjan, Iran
[2]Charles Gerhardt Institute, UMR 5253 CNRS/UM2/ENSCM/UM1, Advanced Materials for Catalysis and Health Group, Higher National School of Chemistry of Montpellier, Montpellier, France
[3]Faculty of Chemistry, University of Kashan, Kashan, Iran

Received: 23.05.2016 • **Accepted/Published Online:** 11.10.2016 • **Final Version:** 19.04.2017

Abstract: Our studies on the selective catalytic reduction of NO (SCR-deNO) properties of M/γ-Al_2O_3 (M = Mn, Co, Cu) nanocatalysts are presented. All catalysts were prepared by homogeneous deposition precipitation using urea as the precursor for the precipitating agent. The SCR activity followed the order Mn/γ-Al_2O_3 > Cu/γ-Al_2O_3 > Co/γ-Al_2O_3. The nanocatalysts were characterized with respect to their texture (N_2-BET), particle size (TEM), reducibility (H_2-TPR), and acidity (NH_3-TPD). The TEM analysis revealed that the metal species have superior dispersion with less agglomeration and sintering on γ-Al_2O_3 support. The H_2-TPR results confirmed that the Mn/γ-Al_2O_3 nanocatalyst contains various oxidation states of manganese, which is useful for the catalyst to maintain the DeNO activities. The NH_3-TPD studies indicated that the addition of transition metal can significantly increase the surface acidity and Mn/γ-Al_2O_3 showed the most adsorbed sites of NH_3. Characterization results indicated that the acidity and the redox properties of the catalyst play important roles in the final catalytic activity in the SCR-NO process.

Key words: NO, NH_3-SCR, transition metals, γ-Al_2O_3, nanocatalyst

1. Introduction

Nitrogen oxides (NO_x = NO + NO_2) are among the main atmospheric pollutants. They are reported to contribute to a variety of environmental problems including acid rain and acidification of aquatic systems, ground level ozone (smog), ozone depletion, visibility degradation and greenhouse effects[1,2] Increasingly stringent limits for exhaust emissions, particularly for nitrogen oxides from lean-burn combustion such as diesel engines, have driven many researchers to look for suitable methods. The selective catalytic reduction (SCR) of NO with ammonia as reductant is the most common method to catalytically reduce NO in flue gases from stationary sources. A number of catalysts consisting of various transition metals on different supporters have been studied for the SCR of NO reaction. Transition metals such as Cu,[3] Co,[4] Fe,[5] and Mn[6,7] have been reported to exhibit high activity. γ-Al_2O_3 has been extensively used as a support in many catalyst formulations, mainly due to its low cost, particular texture, and good thermal stability[8] Torikai et al.[9] studied the performance of alumina catalysts in NH_3-SCR reactions. They reported that the activity improves greatly with the loading of copper and also the addition of copper results in lowering the active temperature region, the higher maximum activity, and the enhancement of the reaction rate. Hamada et al.[10] also investigated the SCR behavior of

*Correspondence: panahi@znu.ac.ir

metal-alumina catalysts and concluded that these catalysts show excellent activity at low temperatures and under high space velocity conditions.

Despite the number of investigations carried out on γ-Al_2O_3-supported transition metal catalysts, there is, to the best of our knowledge, no available study that compares the activity of different transition metals supported on γ-Al_2O_3. Therefore, the goal of this work was the comparison of three catalyst activities (Co/γ-Al_2O_3, Cu/γ-Al_2O_3, and Mn/γ-Al_2O_3) under a common experimental set up and understanding the effect of metal characteristics on NO conversion. Hence, in the present work, metals of cobalt, copper, and manganese were supported on γ-Al_2O_3 by deposition precipitation method and studied for the SCR of NO by ammonia. The effects of transition metals' modification on the microstructure and physiochemical properties were systematically investigated by BET, NH_3-TPD, H_2-TPR, and TEM in combination with the activity evaluation of NO catalytic removal.

2. Results and discussion

2.1. Characterization of catalysts

2.1.1. Analysis of the metal species particle sizes by TEM

The TEM images of the γ-Al_2O_3 and M/γ-Al_2O_3 nanocatalysts are shown in Figures 1a–1d. TEM analysis detected the presence of metal species particles on the γ-Al_2O_3 support. Dark spots are mainly attributed to metal species. For all the nanocatalysts, we can observe the presence of metal species nanoparticles dispersed homogeneously. The coprecipitation method is definitely beneficial for the homogeneous dispersion of metal species deposited at high contents[11] The TEM images also confirmed the nanoscale size of the M/γ-Al_2O_3 catalysts ($<$100 nm).

2.1.2. BET surface area

The BET surface area, pore volume, and pore size of the γ-Al_2O_3 and synthesized M/γ-Al_2O_3 nanocatalysts are summarized in Table 1. The BET surface areas and the pore volume of γ-Al_2O_3 slightly decreased after metal loading, suggesting that the introduction of metal does not obviously affect the textural properties of the support. However, this slight decrease of the BET surface area can be attributed to the partial pore blockage by the metal species.[12] Note, however, that an apparent reduction of the BET surface area may also be caused by the increasing density of the catalysts due to the loading of the support with metal[13] The mean pore diameter has increased with M/γ-Al_2O_3 catalysts in comparison to γ-Al_2O_3. This might be due to dissociation of some bonds in γ-Al_2O_3 because of the urea alkaline environment and consequently the pore diameter is high for M/γ-Al_2O_3 catalysts.

Table 1. BET surface area, pore volume, and average pore diameter of γ-Al_2O_3 and M/γ-Al_2O_3 (M = Cu, Mn, Co) nanocatalysts.

Catalyst	$\gamma-Al_2O_3$	Cu/γ-Al_2O_3	Mn/γ-Al_2O_3	Co/γ-Al_2O_3
BET surface area (m^2/g)	137	124	127	127
Total pore volume (cm^3/g)	0.246	0.237	0.252	0.261
Average pore diameter (Å)	5.6	5.8	6.1	6.2

The overall results by BET analysis of the M/γ-Al_2O_3 nanocatalysts indicated that the introduction of metal species has little effect on the textural properties of γ-Al_2O_3.

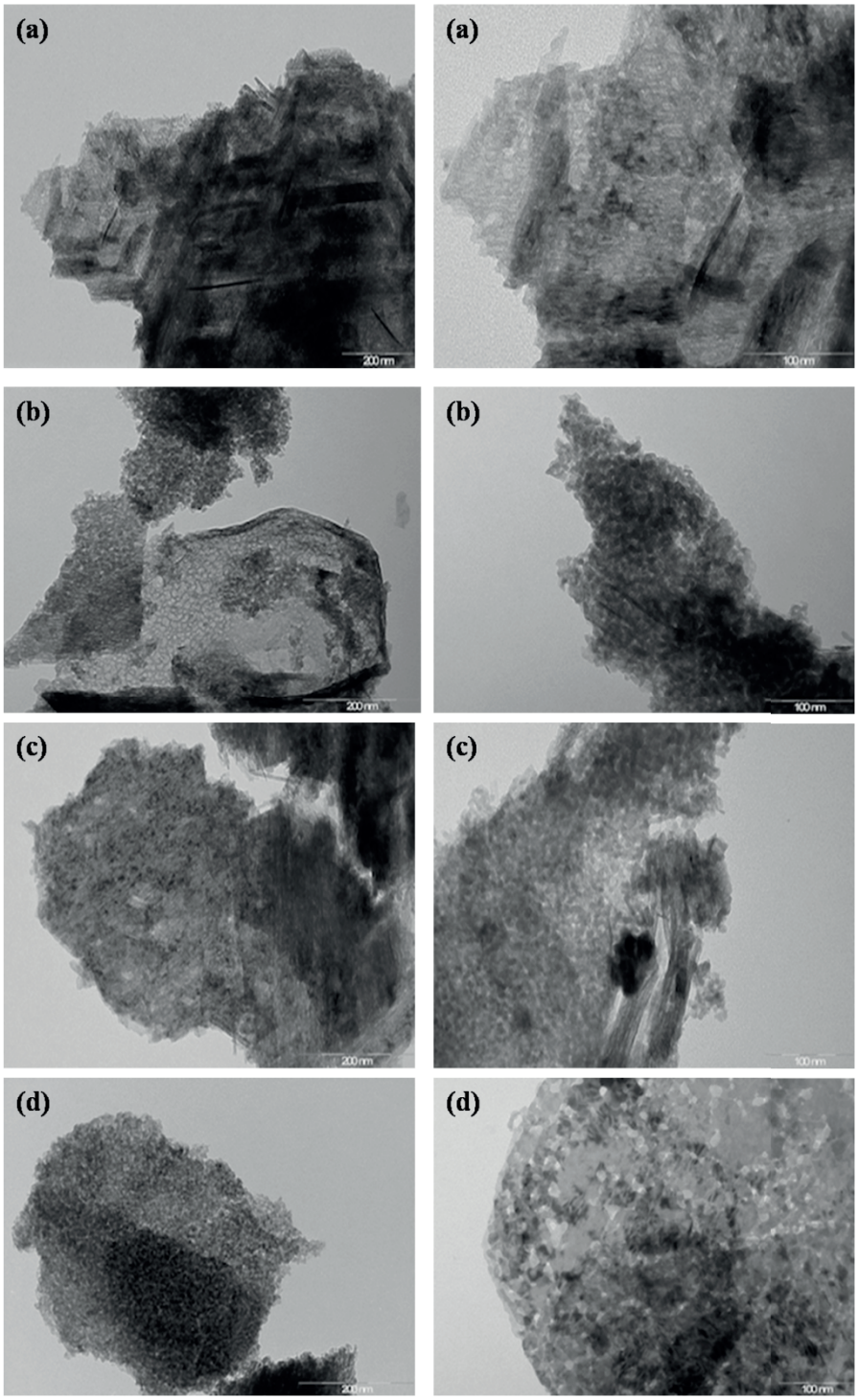

Figure 1. TEM images of (a) γ-Al_2O_3, (b) Cu/γ-Al_2O_3, (c) Mn/γ-Al_2O_3, (d) Co/γ-Al_2O_3.

2.1.3. XRD

The X-ray diffraction patterns of γ-Al_2O_3 and M/γ-Al_2O_3 nanocatalysts are shown in Figure 2. All diffraction peaks corresponding to the γ-Al_2O_3 structure could be clearly observed for all M/γ-Al_2O_3 catalysts,

suggesting that neither the metal loading nor the calcination process significantly affected the γ-Al_2O_3 structure. There were no other peaks in XRD patterns of M/γ-Al_2O_3 nanocatalysts, demonstrating that metal species (e.g., oxides, cations) were well dispersed throughout the γ-Al_2O_3 structure.

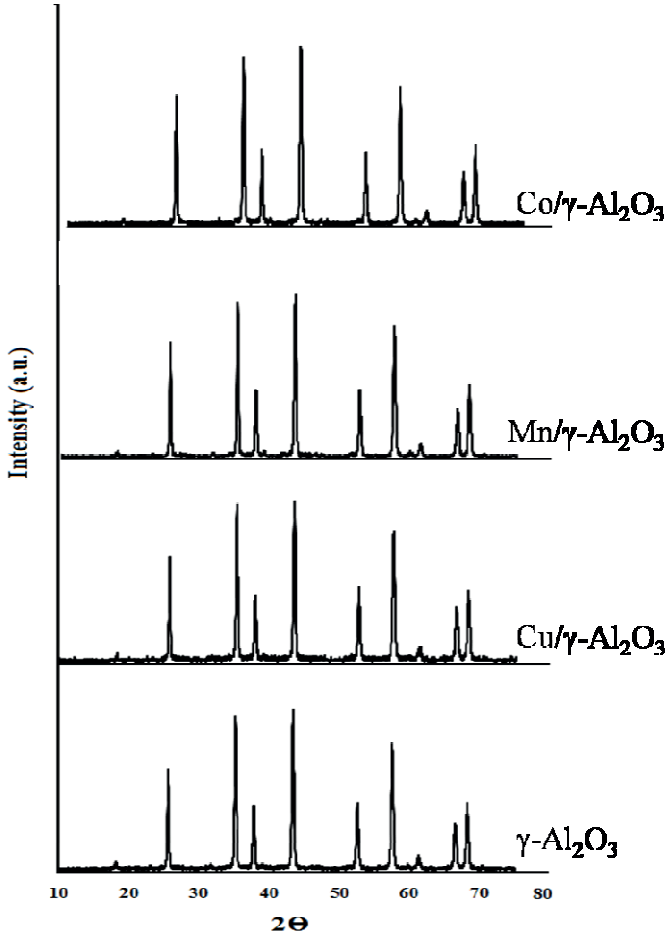

Figure 2. XRD patterns of γ-Al_2O_3 and M/γ-Al_2O_3 nanocatalysts.

2.1.4. Temperature-programmed reduction in H_2 (H_2-TPR)

The reduction property of M/γ-Al_2O_3 nanocatalysts was investigated using H_2-TPR and the results are presented in Figure 3 and Table 2. The Cu/γ-Al_2O_3 catalyst showed one reduction peak around 220 °C. According to results from the literature,[14] this peak can be assigned to the reduction of isolated Cu^{2+} ions to Cu^{+} and possibly also the reduction of nanosized CuO. Three distinct reduction peaks were observed for the Mn/γ-Al_2O_3 catalyst. According to previous studies,[15–17] the low temperature peak at 310 °C is attributed to the reduction of highly dispersed and easily reducible MnO_2 species, the broad middle temperature peak at 430 °C is due to the reduction of Mn_2O_3/Mn_3O_4 or the bulk MnO_x phase, and the high temperature peak with less intensity at 500 °C is due to the reduction of Mn_3O_4/MnO. The reduction process of manganese oxides takes place in the following order: $MnO_2 \rightarrow Mn_2O_3 \rightarrow Mn_3O_4 \rightarrow MnO$[18] Further reduction of MnO to Mn metal is impossible below 800 °C due to its large negative value of reduction potential, which was reported in many studies.[19–21]

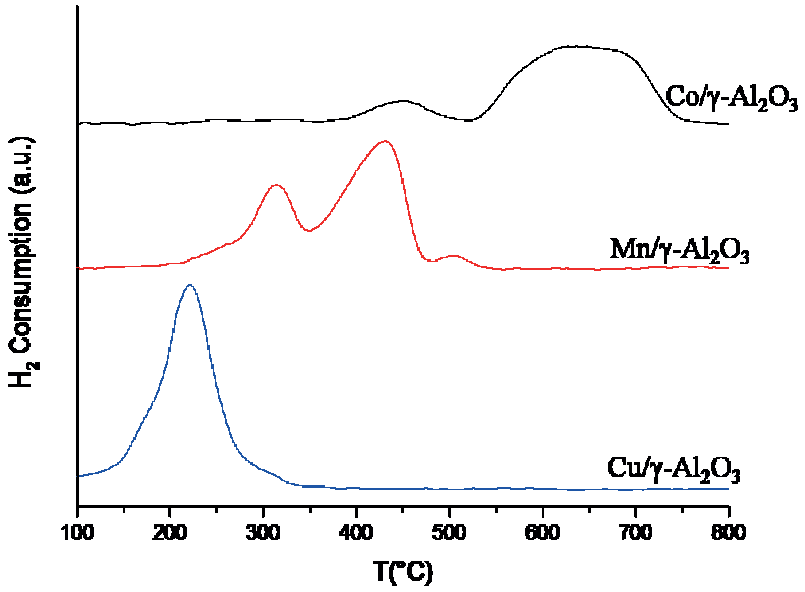

Figure 3. H_2-TPR profiles of M/γ-Al_2O_3 (M = Cu, Mn, Co) nanocatalysts.

Table 2. H_2 consumption during H_2-TPR and acidity obtained from NH_3-TPD in M/γ-Al_2O_3 (M = Cu, Mn, Co) nanocatalysts.

Catalyst	$\gamma-Al_2O_3$	Cu/γ-Al_2O_3	Mn/γ-Al_2O_3	Co/γ-Al_2O_3
Total amount H_2 consumed (μmol/g)	-	432	453	355
Acidity (μmol/g)	151	289	339	247

The Co/γ-Al_2O_3 catalyst showed one main reduction peak at 650 °C, which can be ascribed to the reduction of isolated Co^{2+} ions[22] In addition to the main peak, a small peak at about 450 °C was also observed. This peak corresponds to reduction of cobalt oxo species, such as CoO or Co_3O_4.[23]

A comparison of TPR profiles of M/γ-Al_2O_3 nanocatalysts shows that the Mn/γ-Al_2O_3 catalyst contains various oxidation states of manganese, due to the existence of several reduction peaks. The reduction temperature of copper species in the Cu/γ-Al_2O_3 catalyst (220 °C) was found to be lower than that of cobalt species in the Co/γ-Al_2O_3 catalyst (650 °C), indicating higher reducibility of copper species in Cu/γ-Al_2O_3. The copper species are more easily reducible than cobalt species. The main reduction peak of Co/γ-Al_2O_3 is at a higher temperature in comparison to Mn/γ-Al_2O_3 and Cu/γ-Al_2O_3, implying that the redox activity of the Co/γ-Al_2O_3 catalyst is low. The decrease in the redox property leads to the low activity.

Meanwhile, according to Table 2, the amount of H_2 consumed of Mn/γ-Al_2O_3 (453 μmol/g) is greater than that of Cu/γ-Al_2O_3 (432 μmol/g) and Co/γ-Al_2O_3 (355 μmol/g), implying that the reducing potential of Mn/γ-Al_2O_3 is higher than that of Cu/γ-Al_2O_3 and Co/γ-Al_2O_3.

2.1.5. NH_3 temperature-programmed desorption (TPD) study

To elucidate the role of catalyst acidity, NH_3-TPD was performed on the M/γ-Al_2O_3 catalysts and the γ-Al_2O_3 substrate (Figure 4). γ-Al_2O_3 displayed a broad peak at 100–380 °C. This peak is ascribed to the desorption of weakly bound NH_3, which arises from the physisorbed NH_3 or ammonium species and

also corresponds to the medium-strength acid sites, which is due to the desorption of NH_3 on the Lewis or strong Brønsted acid sites[24] The NH_3-TPD profile of urea-treated γ-Al_2O_3 is similar to γ-Al_2O_3 and it shows that urea does not affect the acidity of alumina. In the case of the M/γ-Al_2O_3 catalysts, the broadened desorption peak and enhanced chemisorbed NH_3 amount suggest that the addition of metal species has remarkably enhanced the concentration and acidity of acid sites[21] Indeed, the addition and high dispersion of metal species increase the acid sites distinctly because metal species generate new Lewis acid sites for NH_3 chemisorption. Additionally, a new distinct NH_3 desorption peak centered at 440 °C emerged for Mn/γ-Al_2O_3, which should be due to the strong Lewis acid sites originating from the high dispersion of the manganese oxide phase[24] The total amount of adsorbed ammonia, which is determined from the area under the TPD curve, is shown in Table 2. For all of the catalysts, the acid site density has increased upon loading with the metal, indicating that new acid sites have been created by metal species. The Mn-containing catalyst exhibited the highest overall density of acid sites (339 μmol/g) among all the catalysts. According to the TPD profiles, the introduction of manganese influences the formation of strong acidic sites in this catalyst. The presence of acid sites is considered to favor NO conversion due to the preferential adsorption of NH_3 on these sites, thus initiating the reaction.[25] Accordingly, one would expect a correlation of the SCR activity with the amount of total acidity (Lewis and Brønsted acidity) and acidic strength (T_{max} of ammonia desorption)[26]

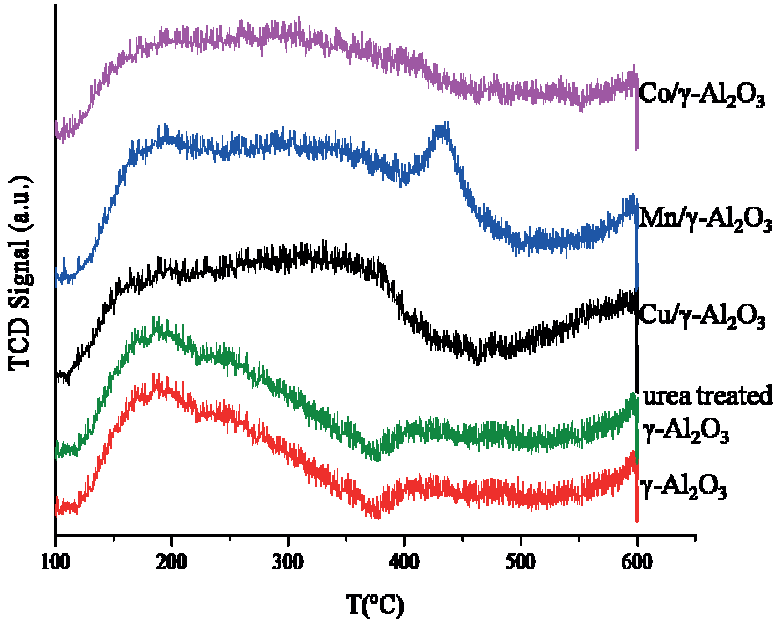

Figure 4. NH_3-TPD profiles of γ-Al_2O_3 and M/γ-Al_2O_3 (M = Cu, Mn, Co) nanocatalysts.

2.2. Catalytic performance

2.2.1. Activity of M/ γ-Al_2O_3 nanocatalysts

The M/γ-Al_2O_3 nanocatalysts were tested as catalysts for the SCR of NO with NH_3. N_2 and N_2O were the only detected N-containing products in the NH_3-SCR process. Figure 5 presents the results of the catalytic studies. The N_2O yield is not addressed here due to its minor value. Moreover, N_2 selectivity was always above 90% for all tested catalysts. As is shown in Figure 5, the NO conversion increases with increasing temperature and reaches nearly 85% at 300 °C for the Mn/γ-Al_2O_3 nanocatalyst.

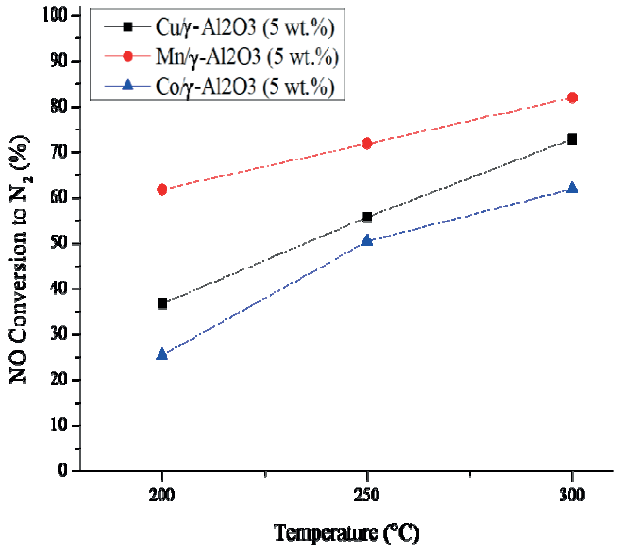

Figure 5. Catalytic performance of M/γ-Al_2O_3 (M = Cu, Mn, Co) nanocatalysts in the NH_3-SCR process.

2.2.2. Correlation between physicochemical properties and catalytic performance

Based on the above results, an attempt to correlate the catalytic performance of metal-promoted γ-Al_2O_3 nanocatalysts in NO catalytic reduction with the physicochemical property of these catalysts was made. According to Figure 5, the Mn/γ-Al_2O_3 catalyst showed better activity and the Co/γ-Al_2O_3 catalyst exhibited the lowest catalytic activity. The TPR results revealed that manganese oxide undergoes the consecutive reduction of $MnO_2 \rightarrow Mn_2O_3 \rightarrow Mn_3O_4 \rightarrow MnO$. The high activity of the Mn/γ-Al_2O_3 catalyst can be attributed to its ability to form variable oxidation states of manganese (MnO_2, Mn_2O_3, Mn_3O_4, and MnO) and its oxygen storage capacity,[27] which is in agreement with the study by Pavani et al[28] Under NH_3-SCR conditions with an excess of O_2, manganese oxides can convert into each other. This works like an electron pump (between NO and NH_3 molecules), enabling a redox cycle to be completed. In order to initiate and continue such a cycle, variable oxidation states of metal seem to be necessary[29]

It is remarkable that Cu/γ-Al_2O_3 exhibited higher activity than Co/γ-Al_2O_3 in the studied temperature range, as shown in Figure 5. This might be related to facile reduction of the copper species as supported by the TPR profiles (see Figure 3)[13] The copper species are more easily reducible than cobalt species. In order to understand the relationship between the number of reducible metal species and the catalytic activity, the peak areas of the TPR profiles were integrated (shown in Table 2). The Mn/γ-Al_2O_3 catalyst showed the most quantitative H_2 consumption, suggesting that this catalyst has the most quantitative available reducibility metal species. The Co/γ-Al_2O_3 catalyst, which exhibited the lowest catalytic activity, showed the least quantitative H_2 consumption.

The chemisorption of NH_3 on acid sites is an important factor for NH_3-SCR reaction. According to NH_3-TPD results, the modification of γ-Al_2O_3 with transition metals caused an increase in the Lewis acid sites. This effect can be related to the electron acceptor behavior of the transition metals, which give rise to additional Lewis acid centers[30] The NH_3-TPD results of catalysts coincide with their catalytic activity. The acid site density of M/γ-Al_2O_3 catalysts (Table 2) matches the changing trend of the NO conversion very well (Figure 5), which means that the more NH_3 molecules the sample adsorbs, the higher the NO conversion of the catalyst is. The Mn-containing catalyst with the highest overall density of acid sites showed the highest NO

conversion. The Cu/γ-Al_2O_3 catalyst also has higher acid site density than the Co/γ-Al_2O_3 catalyst, as a result of which Cu/γ-Al_2O_3 exhibited higher catalytic activity than Co/γ-Al_2O_3. Suprun et al.[31] announced that the activity increases with the acid site density for mesoporous materials. Another reason for the highest efficiency of the Mn/γ-Al_2O_3 nanocatalyst could be the availability of more and stronger NH_3 adsorption sites, which are deduced to correlate with the catalytically active sites. The results of NH_3-TPD can also explain the low NO conversion exhibited by the Co/γ-Al_2O_3 catalyst. With investigation of the reports on the topic, it can be concluded that Mn/γ-Al_2O_3 prepared by the homogeneous deposition precipitation (HDP) method has better low temperature activity than some manganese supporting other materials for SCR of NO in the literature[26,32]

In conclusion, cobalt, copper, and manganese oxide nanocatalysts supported on γ-Al_2O_3 were prepared by the HDP method and activity of these catalysts was investigated in NH_3-SCR of the NO process. The experimental results showed that Mn/γ-Al_2O_3 has the best catalytic activity, which was above 60% at the temperature range between 200 and 300 °C. The nanocatalysts were characterized by BET, TEM, H_2-TPR, and NH_3-TPD. The TEM images indicated that metal species as nanoparticles with homogeneous dispersion were present on the γ-Al_2O_3 support. The NH_3-TPD analysis indicated that introduction of transition metals generated additional strong Lewis centers for ammonia adsorption with M/γ-Al_2O_3 catalysts. From both the NH_3-TPD and H_2-TPR results, it was concluded that the Mn/γ-Al_2O_3 nanocatalyst offered the most and strongest adsorbed sites of NH_3 species and variable oxidation states of manganese; consequently, it had the best catalytic activity among the catalysts. Furthermore, the Co/γ-Al_2O_3 catalyst exhibited the lowest activity because the redox activity of this catalyst is low and also it has fewer acid sites.

3. Experimental

3.1. Nanocatalyst preparation

According to a previous study,[33] the preparation method of HDP using urea enables the even deposition of metal species. Therefore, metal-based alumina catalysts were prepared by HDP using urea as the precursor for the precipitating agent. $Cu(NO_3)_2.3H_2O$, $Co(NO_3)_2.6H_2O$, and $Mn(NO_3)_2.4H_2O$ were used as precursors. Typically, an appropriate amount of metal nitrate was dissolved in distilled water, and 1 g of γ-Al_2O_3 support was added to the solution with stirring. The amount of metal in the solution corresponds to metal loading of 5 wt.% on γ-Al_2O_3. To this mixture solution, urea was added under vigorous stirring, and the temperature was gradually increased to 95 °C and maintained for 5 h until the hydroxide precipitate was completed. The resulting mixture was aged for 14 h at room temperature and then was filtered, followed by several washings with distilled water to attain a neutral pH. The resulting precipitate was dried in an oven for 12 h and subsequently calcined at 550 °C for 4 h in air.[34]

3.2. Nanocatalyst characterization

The nature, reducibility, and amount of metal species were estimated by H_2-TPR. The experiments were carried out with a Micromeritics 2910 apparatus using H_2/Ar (3/97, v/v) gas at a total flowrate of 15 cm^3 min^{-1} and by heating the samples from 50 to 900 °C (10 °C min^{-1}). In each case, 0.051 g of the catalyst was previously activated at 500 °C for 30 min under air, and then cooled to 50 °C under 20% O_2 in He. TPR with H_2/Ar (3/97, v/v) was then started and the thermal conductivity detector continuously monitored the H_2 consumption.

The acidity of the catalysts was measured by NH_3-TPD technique. Before NH_3 adsorption, the samples were pretreated at 500 °C for 30 min in air and then cooled to 100 °C under 20% O_2 in He, followed by ammonia adsorption with 5% NH_3/He mixture (flowrate: 40 cm^3 min^{-1}) at 100 °C for 30 min. Subsequently, the sample was subjected to He flow (flowrate: 25 cm^3 min^{-1}) for 30 min at 100 °C to remove physically adsorbed ammonia. Ammonia desorption was carried out by raising the temperature to 550 °C with a heating rate of 10 °C min^{-1}.

The textural properties of the catalysts were obtained from nitrogen adsorption–desorption isotherms measured at –196 °C with a Micromeritics ASAP 2000 Analyzer. Before the nitrogen adsorption measurement, the samples were outgassed at 250 °C until a static vacuum of 3×10^{-5} bar was reached. The BET method was used to calculate the specific surface area, whereas the pore size and volume were estimated using the T-plot method.

TEM images of the catalysts were obtained to give an indication of the metal species' size and their dispersion on the support. The samples were ground with a mortar, and then about 1 mg of solid was dispersed in ethanol (about 3 mL) by sonication. A drop of the dispersion was then deposited on a copper grid covered with a Formvar carbon film.

X-ray diffraction (XRD, D 500 Siemens diffractometer, Cu Kα radiation) was utilized to determine the crystal phase and dispersion of the metal species on the γ-Al_2O_3 support. The powdered samples were pressed onto suitable holders and scanned within the 2? range of 5° to 75° with a scanning rate of 0.016 s^{-1}.

3.3. Catalytic conversion of NO with NH_3

The de-NO activity measurements of prepared nanocatalysts were carried out at atmospheric pressure in a fixed bed reactor. In each run, a measured amount of powdered catalyst (0.2 g) was spread between quartz wool in the reactor, and then the reactor was placed inside in a furnace that is electrically heated. Before the catalytic tests, the catalysts were heated up 200 °C and kept at this temperature for 1 h in flowing Ar (100 cm^3 min^{-1}) in order to eliminate possible compounds adsorbed on the catalyst surface. Subsequently, a gaseous reactant feed consisting of 1000 ppm NO, 1000 ppm NH_3, and 5 vol.% O_2 in Ar as the carrier gas was directed over the catalyst. The overall gas flowrate was 150 cm^3 min^{-1} (GHSV = 12,000 h^{-1}) and the experiments were performed at 200–300 °C. Effluent gases after reaching a steady state were analyzed by gas chromatography (Shimadzu model 2010 Plus, TCD detector) equipped with a Molecular Sieve 5A column to separate N_2 (as the selective product) and N_2O (as the nonselective product). The catalytic activity for NO removal was evaluated by the extent of NO conversion into N_2 using the following equation:

$$NO \text{ Conversion to } N_2\% = \frac{[N_2]_{out}}{[NO]_{in}} \times 100$$

The subscripts *in* and *out* indicate the inlet and outlet concentrations at steady state, respectively.

Acknowledgment

The authors would like to acknowledge the financial support from the University of Tabriz, University of Zanjan, and the Iranian Nanotechnology Initiative.

References

1. Bosch, H., Janssen, F. *Catal. Today* **1988**, *2*, 369-379.
2. Skalska, K.; Miller, J. S.; Ledakowicz, S. *Sci. Total Environ.* **2010**, *408*, 3976-3989.
3. Amanpour, J.; Salari, D.; Niaei, A.; Mousavi, S. M.; Nakhostin Panahi, P. *J. Environ. Sci. Heal. A* **2013**, *48*, 879-886.
4. Nakhostin Panahi, P.; Niaei, A.; Tseng, H. H.; Salari, D.; Mousavi, S. M. *Neural Comput. Appl.* **2015**, *26*, 1515-1523.
5. Mousavi, S. M.; Niaei, A.; Illán Gómez, M. J.; Salari, D.; Nakhostin Panahi, P.; Abaladejo-Fuentes, V. *Mater. Chem. Phys.* **2014**, *143*, 921-928.
6. Mousavi, S. M.; Niaei, A.; Salari, D.; Panahi, P. N.; Samandari, M. *Environ. Technol.* **2013**, *34*, 1377-1384.
7. Mousavi, S. M.; Salari, D.; Niaei, A.; Nakhostin Panahi, P.; Shafiei, S. *Environ. Technol.* **2014**, *35*, 581-589.
8. Ayari, F.; Mhamdi, M.; Delahay, G.; Ghorbel, A. *J. Porous Mater.* **2010**, *17*, 265-274.
9. Torikai, Y.; Yahiro, H.; Mizuno, N.; Iwamoto, M. *Catal. Lett.* **1991**, *9*, 91-95.
10. Hamada, H.; Kintaichi, Y.; Sasaki, M.; Ito, T.; Tabata, M. *Appl. Catal.* **1991**, *75*, L1-L8.
11. Zhang, F.; Zhang, S.; Guan, N.; Schreier, E.; Richter, M.; Eckelt, R.; Fricke, R. *Appl. Catal. B.* **2007**, *73*, 209-219.
12. Pereda-Ayo, B.; De La Torre, U.; Illán-Gómez, M. J.; Bueno-López, A.; González-Velasco, J. R. *Appl. Catal. B* **2014**, *147*, 420-428.
13. Worch, D.; Suprun, W.; Gläser, R. *Catal. Today* **2011**, *176*, 309-313.
14. Wijayanti, K.; Andonova, S.; Kumar, A.; Li, J.; Kamasamudram, K.; Currier, N. W.; Yezerets, A.; Olsson, L. *Appl. Catal. B* **2015**, *166-167*, 568-579.
15. Zhang, Q.; Qiu, C.; Xu, H.; Lin, T.; Lin, Z.; Gong, M.; Chen, Y. *Catal. Today* **2011**, *175*, 171-176.
16. Ettireddy, P. R.; Ettireddy, N.; Mamedov, S.; Boolchand, P.; Smirniotis, P. G. *Appl. Catal. B* **2007**, *76*, 123-134.
17. Liu, F.; He, H.; Ding, Y.; Zhang, C. *Appl. Catal. B* **2009**, *93*, 194-204.
18. Cao, F.; Su, S.; Xiang, J.; Wang, P.; Hu, S.; Sun, L.; Zhang, A. *Fuel* **2015**, *139*, 232-239.
19. Tang, X.; Li, Y.; Huang, X.; Xu, Y.; Zhu, H.; Wang, J.; Shen, W. *Appl. Catal. B* **2006**, *62*, 265-273.
20. Trawczyński, J.; Bielak, B.; Miśta, W. *Appl. Catal. B* **2005**, *55*, 277-285.
21. Wan, Y.; Zhao, W.; Tang, Y.; Li, L.; Wang, H.; Cui, Y.; Gu, J.; Li, Y.; Shi, J. *Appl. Catal. B* **2014**, *148-149*, 114-122.
22. Lónyi, F.; Solt, H. E.; Valyon, J.; Boix, A.; Gutierrez, L. B. *Appl. Catal. B* **2012**, *117-118*, 212-223.
23. Horiuchi, T. F., Chen, L.; Suzuki, K.; Mori, T. *Catal. Lett.* **2002**, *78*, 319-323.
24. Cao, F.; Xiang, J.; Su, S.; Wang, P.; Hu, S.; Sun, L. *Fuel Process. Technol.* **2015**, *135*, 66-72.
25. Yang, S.; Wang, C.; Li, J.; Yan, N.; Ma, L.; Chang, H. *Appl. Catal. B* **2011**, *110*, 71-80.
26. Putluru, S. S. R.; Schill, L.; Jensen, A. D.; Siret, B.; Tabaries, F.; Fehrmann, R. *Appl. Catal. B* **2015**, *165*, 628-635.
27. Craciun, R.; Nentwick, B.; Hadjiivanov, K.; Knözinger, H. *Appl. Catal. A* **2003**, *243*, 67-79.
28. Sreekanth, P. M.; Smirniotis, P. G. *Catal. Lett.* **2007**, *122*, 37-42.
29. Ochońska, J.; McClymont, D.; Jodłowski, P. J.; Knapik, A.; Gil, B.; Makowski, W.; Łasocha, W.; Kołodziej, A.; Kolaczkowski, S. T.; Łojewska, J. *Catal. Today* **2012**, *191*, 6-11.
30. Chmielarz, L.; Kuśtrowski, P.; Dziembaj, R.; Cool, P.; Vansant, E. F. *Catal. Today* **2007**, *119*, 181-186.
31. Suprun, W.; Schaedlich, K.; Papp, H. *Chem. Eng. Technol.* **2005**, *28*, 199-203.
32. De Lucas, A.; Valverde, J.; Dorado, F.; Romero, A.; Asencio, I. *J. Mol. Catal. A-Chem.* **2005**, *225*, 47-58.
33. Nakhostin Panahi, P.; Salari, D.; Tseng, H. H.; Niaei, A.; Mousavi, S. M. *Environ. Technol.* (in press).
34. Choudhary, V. R.; Dumbre, D. K.: *Catal. Commun.* **2009**, *10*, 1738-1742.